npj | quantum materials

Article

Published in partnership with Nanjing University

https://doi.org/10.1038/s41535-024-00636-4

Field-controlled multicritical behavior and emergent universality in fully frustrated quantum magnets

Yuchen Fan[1], Ning Xi[2], Changle Liu[3,4], Bruce Normand[5,6] ✉ & Rong Yu[2,7] ✉

Phase transitions in condensed matter are a source of exotic emergent properties. We study the fully frustrated bilayer Heisenberg antiferromagnet to demonstrate that an applied magnetic field creates a previously unknown emergent criticality. The quantum phase diagram contains four states with distinctly different symmetries, all but one pair separated by first-order transitions. We show by quantum Monte Carlo simulations that the thermal phase diagram is dominated by a wall of discontinuities extending between the dimer-triplet phases and the singlet-containing phases. This wall is terminated at finite temperatures by a critical line, which becomes multicritical where the Berezinskii-Kosterlitz-Thouless (BKT) transition of the dimer-triplet antiferromagnet and the thermal Ising transition of the singlet-triplet crystal phase also terminate. The combination of merging symmetries leads to a 4-state Potts universality not contained in the microscopic Hamiltonian, which we interpret within the Ashkin-Teller model. Our results represent a systematic step in understanding emergent phenomena in quantum magnetic materials, including the "Shastry-Sutherland compound" $SrCu_2(BO_3)_2$.

Classical and quantum field theories, formulated to capture the low-energy, long-wavelength behavior of a system, have a foundational role in theoretical physics. At a continuous classical or quantum phase transition (QPT), the characteristic energy scale vanishes and the correlation length diverges, ensuring a profound connection between field theories and the statistical mechanics of critical phenomena[1]. In both situations, the microscopic details become irrelevant and the critical properties of the system are dictated only by global and scale-invariant characteristics such as the dimensionality, symmetry, and sometimes the topology. Because these most basic attributes are all discrete, field theories are readily classified and phase transitions can be categorized by their universality class.

One of the organizing principles of modern condensed matter is the concept of "emergence," meaning large-scale patterns of behavior that cannot be predicted from a knowledge of the short-range interactions. Quantum magnetic materials and models are widely recognized for the wealth of emergent phenomena they exhibit at low energies, which include multiple types of fractional excitation and of quantum spin liquid[2]. Many more phenomena emerge when a system is driven into the critical regime around a phase transition[3]. Beyond the continuous (second-order) transitions that are now well studied in experiment[4,5], theory predicts that the order parameters of two phases with unrelated symmetries can vanish continuously and simultaneously. This deconfined quantum critical point (DQCP)[6,7], or multicritical point[8,9], should be accompanied by emergent fractional excitations, exhibit unconventional critical scaling[10], and possess an enhanced continuous symmetry. More generally, emergent enhanced symmetries have recently been discussed at a first-order transition[11] and at topological phase transitions[12,13].

The many-body states of quantum spin systems can be altered by a variety of experimental methods, including an applied magnetic field[4], a hydrostatic pressure[5,14], and controlled substitional disorder[15], to obtain a wide range of possibilities for the investigation of phase transitions and related emergent phenomena. The field-induced magnetic order observed in dimerized spin systems can be described as a Bose-Einstein condensation of triplet excitations into the singlet ground state[4], while the

[1]Beijing National Laboratory for Condensed Matter Physics and Institute of Physics, Chinese Academy of Sciences, Beijing 100190, China. [2]Department of Physics and Beijing Key Laboratory of Opto-electronic Functional Materials and Micro-nano Devices, Renmin University of China, Beijing 100872, China. [3]School of Engineering, Dali University, Dali, Yunnan 671003, China. [4]Shenzhen Institute for Quantum Science and Technology and Department of Physics, Southern University of Science and Technology, Shenzhen 518055, China. [5]Laboratory for Theoretical and Computational Physics, Paul Scherrer Institute, CH-5232 Villigen-PSI, Switzerland. [6]Institute of Physics, Ecole Polytechnique Fédérale de Lausanne (EPFL), CH-1015 Lausanne, Switzerland. [7]Key Laboratory of Quantum State Construction and Manipulation (Ministry of Education), Renmin University of China, Beijing 100872, China. ✉e-mail: bruce.normand@psi.ch; rong.yu@ruc.edu.cn

pressure-induced transition[5] is a triplet condensation in the 3D XY universality class. It was pointed out recently that critical phenomena in quantum magnets are not restricted to second-order QPTs, but that the combination of quantum and thermal fluctuations can produce a critical point when the QPT is first-order[16]. Using the $S = 1/2$ "fully frustrated bilayer" (FFB) model shown in Fig. 1a, it was found that the discontinuity across the QPT, between the dimer-singlet and dimer-triplet phases (DS and DTAF in Fig. 1b), decreases with increasing temperature and terminates at a finite-temperature critical point. In this minimal model, there is no spontaneous symmetry-breaking across the line of discontinuities (meaning at $T > 0$, by the Mermin-Wagner theorem) and the extent of singlet-triplet order provides a quantum magnetic analog of the liquid-gas transition, the two-component nature conferring an Ising universality[17].

This type of physics and its extensions have recently been pursued in a number of frustrated quantum spin models[18–20], but came to the fore when it was shown to be the origin of critical-point behavior found[21] in specific-heat measurements on the frustrated quantum antiferromagnet $SrCu_2(BO_3)_2$. This compound provides a remarkably faithful realization of the Shastry-Sutherland model (SSM)[22], not only at ambient pressure[23] but also in its pressure-induced QPTs[14]. However, the first-order QPT in $SrCu_2(BO_3)_2$ and the SSM separates a DS phase from a plaquette-singlet phase, which does have long-ranged order at low temperatures and a continuous thermal transition[21], making the situation more complex than the FFB. In an applied magnetic field, $SrCu_2(BO_3)_2$ shows a spin-nematic phase[24] followed by a complex cascade of QPTs into different magnetization-plateau states[23,25], raising important questions about the nature of criticality under combined fields and pressures. The possibilities range from emergent enhanced symmetries and emergent types of multicriticality to the appearance of a DQCP suggested by theory[26], numerics[27], and experiment[28].

Here we look more deeply into the FFB model to study how its phases and phase transitions evolve in an applied magnetic field. The field enriches the phase diagram, turning the dimer-triplet state into a Berezinskii-Kosterlitz-Thouless (BKT) phase with quasi-long-ranged order (qLRO) and the DS state into a checkerboard triplon crystal (TC) phase with LRO at finite temperatures. The Ising critical point becomes a critical line, first retaining its Ising character but then gaining an emergent 4-state Potts symmetry on the multicritical phase boundary to the TC regime, before terminating at a quantum critical endpoint (QCEP). All our thermal calculations are performed using large-scale quantum Monte Carlo (QMC) methods enabled by the recent qualitative breakthrough that the fully frustrated system formulated in the dimer basis has no sign problem. We map the quantum FFB model to a classical equivalent and then to the Ashkin-Teller model in order to trace the origin of emergent criticality, and hence to shed light on its possible appearance in highly frustrated quantum magnetic materials such as $SrCu_2(BO_3)_2$.

Results

FFB Model

The Hamiltonian of the FFB model is

$$\mathcal{H} = \sum_i J_\perp \vec{S}_{i,1} \cdot \vec{S}_{i,2} - H \sum_{i,m=1,2} S^z_{i,m} + \sum_{\langle i,j\rangle,m=1,2} \left[J_\parallel \vec{S}_{i,m} \cdot \vec{S}_{j,m} + J_\times \vec{S}_{i,m} \cdot \vec{S}_{j,\bar{m}} \right], \quad (1)$$

where $\vec{S}_{i,m}$ is a quantum ($S = 1/2$) spin at site i and layer m of the square-lattice bilayer shown in Fig. 1a, H is the applied magnetic field, and the antiferromagnetic (AF) Heisenberg interactions are $J_\perp$ on the interlayer

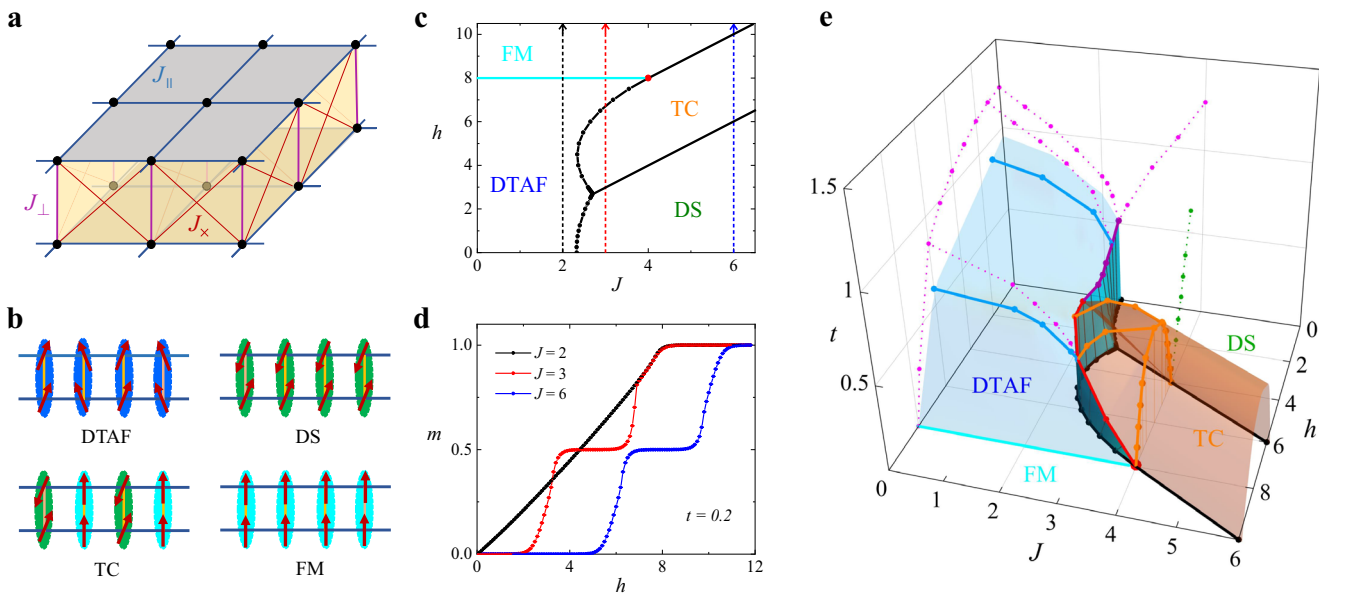

Fig. 1 | Phase diagram of the fully frustrated bilayer Heisenberg model in an applied magnetic field. a FFB model. Quantum spins ($S = 1/2$) are located at every site of a pair of square lattices. The interlayer dimer unit has magnetic interaction $J_\perp$, the intralayer interaction is $J_\parallel$, and the interlayer interaction between adjacent sites is $J_\times$; all three interactions are antiferromagnetic (AF) and of Heisenberg type. **b** Representations of the four different ground states in an applied field, the dimer triplet antiferromagnet (DTAF), dimer singlet (DS), checkerboard triplon crystal (TC), and fully polarized ferromagnet (FM). **c** Ground-state phase diagram obtained by the iPESS method. Apart from the field-driven DTAF-FM transition (cyan line), which is continuous, all other transitions are first-order (black lines). The red circle marks the quantum critical endpoint (QCEP) at $J = 4$ and $h = 8$. **d** Magnetization shown as a function of J at low temperature ($t = 0.2$), calculated by quantum Monte Carlo (QMC) for a system of size $L \times L$ dimers, with $L = 24$. The half-magnetization plateau characterizes the TC state. **e** Thermal phase diagram. Long-ranged DTAF and FM order is present only at zero temperature. The TC order parameter persists at finite temperatures, and this order melts continuously at the orange surface. The wall of discontinuities in the triplet density that separates the DTAF and DS phases terminates at a line of Ising critical points (purple) at finite temperatures, while the wall separating the DTAF and TC phases terminates at a line of emergent multicritical points (red). Each point on the red line is simultaneously the endpoint of a BKT transition of the DTAF (blue line with stars) and of a thermal Ising transition of the TC (orange), and exhibits an emergent 4-state Potts criticality. At high fields, the line of emergent multicritical points terminates at the QCEP (red circle). The magenta and green dashed lines mark characteristic crossover temperatures determined by computing the specific heat. Error bars on the phase-boundary points in panels c and e are smaller than the symbol sizes.

dimer bond, $J_\parallel$ within each square lattice, and $J_\times$ between next-neighbor interlayer sites, which frustrates $J_\parallel$. We consider only the fully frustrated case, $J_\times = J_\parallel$, where the model can be rewritten in the dimer basis as

$$\mathcal{H} = J_\parallel \sum_{i,j} \vec{T}_i \cdot \vec{T}_j + J_\perp \sum_i \left(\frac{1}{2} \vec{T}_i^{\,2} - \frac{3}{4} \right) - H \sum_i T_i^z, \qquad (2)$$

with $\vec{T}_i = \vec{S}_{i,1} + \vec{S}_{i,2}$ the total spin of each dimer; $\vec{T}_i^{\,2}$ is proportional to the spin-triplet density and is locally conserved, meaning on every dimer, *i*. This is the property that causes the sign problem, which conventionally accompanies QMC simulations on frustrated spin systems, to be completely absent[29,30]. Thus we can use the stochastic series expansion (SSE) algorithm[31] to obtain highly accurate simulation results for square-lattice dimensions $L \times L$ up to a linear size of $L = 40$. We take $J_\parallel$ as the unit of energy and define the reduced coupling $J = J_\perp/J_\parallel$, reduced field $h = H/J_\parallel$, and reduced temperature $t = T/J_\parallel$, with the lowest temperature we access being $t = 0.1$. To complement these thermal results, we calculate the quantum ($t = 0$) phase diagram of the FFB in a field by applying the tensor-network method of infinite Projected Entangled Simplex States (iPESS)[32] as summarized in the Methods section.

The FFB model has been studied in detail by SSE QMC at zero field[16], and our aim here is to reveal the complex and emergent phenomena induced by the magnetic field. Some properties of the FFB in a field have been investigated by Derzhko, Krokhmalski, Richter, and coworkers in a series of studies[33–35]. These authors drew attention to the fact that the class of fully frustrated models has maximally localized spin excitations (magnons, to which we refer due to their local rung-triplet nature as triplons), and hence completely flat bands. The action of the magnetic field on this rather simple excitation spectrum is a systematic alteration of the energies of the different multiplets, leading to clear field-controlled level-crossings of macroscopic numbers of states. These authors also studied the use of classical lattice-gas models to analyze the physics of these quantum spin systems, but did not discuss the full phase diagram or emergent critical properties.

Quantum Phase Diagram

We begin by using iPESS to identify the four ground states of the model illustrated schematically in Fig. 1b. A straightforward energy comparison, described in Supplementary Note 1, yields the $t = 0$ phase diagram shown in Fig. 1c. The DS and dimer-triplet antiferromagnet (DTAF) phases are familiar at zero field. Beyond a finite field, the DS is driven into the intermediate TC state, of alternating dimer singlets and field-aligned triplets, and the magnetization shows a plateau at half of its saturation value (Fig. 1d)[34]. Sufficiently strong fields cause a full polarization of the DTAF and TC phases into the FM state. Because only the DTAF and FM phases have the same triplet density ($n_t = 1$), every phase boundary in Fig. 1c is first-order, other than the line of continuous DTAF-FM transitions. This line terminates at a QCEP at $J = 4$ and $h = 8$, where it meets the first-order phase boundary of the TC state.

Figure 1e shows the thermal phase diagram we obtain from our SSE QMC simulations. Only the TC phase has LRO, which is terminated at a thermal transition (orange surface), although the DTAF has qLRO that is lost at a BKT transition (blue). The first-order DS-TC and TC-FM transitions become continuous at any finite temperature, an unconventional property we give the simple terminology "zero-temperature first-order line." The first-order DTAF-DS and DTAF-TC lines persist to finite temperatures, forming a wall of discontinuities across the phase diagram, which is terminated by a (multi)critical line whose nature is the primary focus of our work.

DS and TC phases

To analyse the rich variety of phenomena on display in Fig. 1e, we start on the DS side by considering the field-induced behavior at fixed $J = 4$ (Fig. 2a). The DS phase has no order parameter, but can be characterized by the dimer spin correlation[21]. At finite fields, the average of the three Zeeman-split triplon branches determines the position of the broad maximum in the specific heat (Fig. 2b), while the closure of the gap to the lowest triplon sets the DS-TC transition, shown in Fig. 1c. At $J = 4$ and $t = 0$, the ground state undergoes first-order transitions from DS to TC at $h = 4$ and TC to FM at $h = 8$, where the TC phase supports true LRO and thus has a continuous thermal phase transition at any point on the orange surface in Fig. 1e. By the scaling-collapse analysis presented in Fig. 2c and described in the Methods section, we show that this transition has the critical exponents of Ising universality, $\nu = 1$ and $\beta = 1/8$, as might be anticipated from the twofold degeneracy (i.e. broken Z_2 sublattice symmetry) of the checkerboard TC state.

We reiterate the curious nature of the critical surface of the TC phase at the DS and FM transitions, which changes from second- to first-order precisely at $t = 0$. The termination of a second-order line on a first-order one is known as a critical endpoint[36,37], and a second-order line turning first-order is a tricritical point, but the DS-TC and TC-FM boundaries lack a first-order surface (*cf.* the QCEP at ($J = 4$, $h = 8$)) or half-surface; thus we use instead the term zero-temperature first-order line. The physics of the DS-TC line is that any state excluding nearest-neighbor triplon pairs minimizes the energy, resulting in a highly degenerate ground state[33–35]. Away from the line, these states form low-energy excitations, while excitations containing at least one triplon pair have a gap of order $J_\parallel$, and these two types of process account for the two peaks in $C(t)$ (Fig. 2b). Exactly analogous behavior is observed around the TC-FM line as a consequence of particle-hole symmetry about $n_t = 1/2$. By contrast, the TC-DTAF transition remains first-order up to a finite temperature, where the TC surface meets the line of critical points to establish the emergent criticality we analyse below.

Quantum Critical Endpoint

Finally, to investigate the QCEP, defined as the termination point of a line of continuous QPTs (the DTAF-FM line), we characterize the low-energy excitation spectrum by computing the thermal energy, $E(t) - E_0$, at different points on the zero-temperature first-order lines. As Fig. 2d shows for the two transitions at $J = 6$, $E(t)$ has the same exponential form, indicating gapped excitations above the ground manifold, with the same prefactor, thereby respecting the particle-hole symmetry. However, in Fig. 2e we observe a departure from this symmetry when the QCEP is compared to its counterpart ($h = 4$), with additional thermal energy at $t \lesssim 0.5$ suggesting low-energy AF spin-wave fluctuations, in finite-sized regimes of the neighboring DTAF phase, appearing within the gap.

DTAF phase

Turning to the DTAF side of the phase diagram (Fig. 1e), the field breaks the SU(2) spin symmetry down to U(1) and the DTAF phase supports qLRO below a finite-temperature BKT transition[38,39]. In Fig. 3a we use the specific heat to show that the thermodynamic properties of the DTAF phase, computed at $h = 6$ for a number of J values, remain similar to those at $h = 0$, with a single peak marking a characteristic crossover temperature. An accurate determination of t_{KT} can be obtained[40,41] from the finite-size scaling of the spin stiffness, $\rho_s(t)$, as we explain in the Methods section and show in Fig. 3b, c. As expected[17], t_{KT} is not reflected in the conventional thermodynamic response (Fig. 3a), lying systematically beneath the crossover such that the two temperatures form two sets of surfaces that meet along the line of (multi)critical points (Fig. 1e); in Supplementary Note 2 we show further data illustrating this situation in the DTAF phase.

Critical Line

Given the qLRO of the DTAF phase below t_{KT}, and the LRO of the TC phase below a transition that also appears to converge on the critical line, the crucial question arises of how these field-induced phases affect the universality. We preface the discussion to follow with an important remark: we have found in Fig. 4a–c that all the transition and crossover lines meet with an accuracy of 0.01 in our units, as we show in Supplementary Note 2.

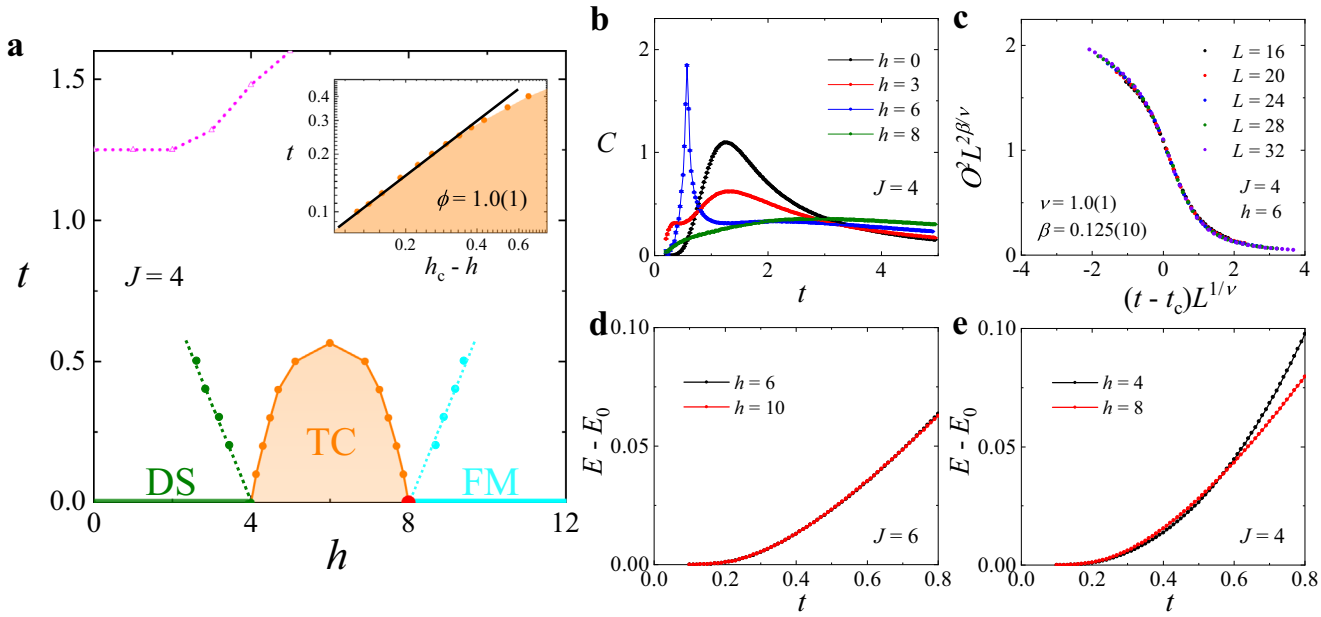

Fig. 2 | Physics of the DS and TC phases, and at the QCEP. a (h, t) phase diagram of the FFB model at $J = 4.0$. Error bars are smaller than the symbol sizes. The dashed green line shows the gap of the DS phase, the dashed cyan line the FM gap, the dashed magenta line the characteristic crossover temperature determined from the specific heat, and the solid orange line the TC ordering temperature. The inset shows that the field-scaling exponent is $\phi = 1$; the model does not have 2+1D Ising universality because the $t = 0$ transition is first-order. **b** Specific heat, $C(t)$, shown for a number of applied field values. The peak temperatures are used to determine the phase-boundary (orange) and crossover lines (magenta) in panel **a**. **c** Ising nature of the thermal transition of the TC phase, shown by scaling collapse of the order parameter, $O(t, L)$, calculated at $J = 4$ and $h = 6$ for systems of linear size L. The critical exponents are fully compatible with the Ising values $\nu = 1$ and $\beta = 1/8$. **d** Thermal energy, $E(t) - E_0$, computed with $L = 24$ and shown at the points $(J, h) = (6, 6)$ and $(J, h) = (6, 10)$, which lie respectively on the zero-temperature first-order DS-TC and TC-FM lines. The exponential form arises due to the gapped nature of both phases and appears identical as a consequence of particle-hole symmetry about triplet density $n_t = 1/2$. **e** $E(t) - E_0$ at the points $(J, h) = (4, 4)$, on the DS-TC zero-temperature first-order line, and $(J, h) = (4, 8)$, which is the QCEP. The change in exponential form indicates a violation of particle-hole symmetry due to the presence of low-energy spin-wave excitations at the QCEP.

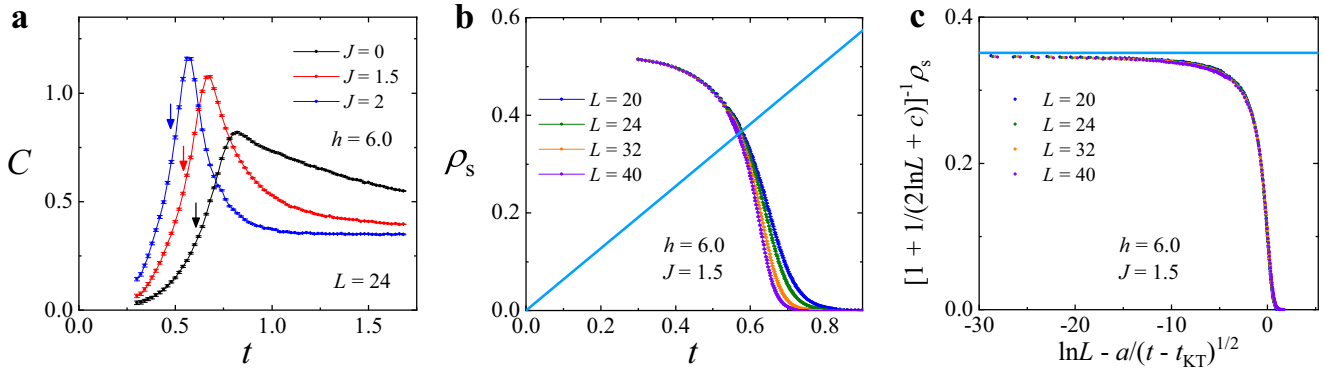

Fig. 3 | Physics of the DTAF phase. a Thermodynamic properties of the DTAF, illustrated by the specific heat, $C(T)$, at $h = 6$ for three different J values. The center of the single broad peak gives a characteristic crossover temperature that lies above the BKT transition (colored arrows). **b** Spin stiffness, $\rho_s(t)$, computed for systems of different sizes, L, at $h = 6$ and $J = 1.5$. The BKT transition temperature, t_{KT}, is determined from the crossing point of $\rho_s(t)$ with the linear function $2t/\pi$ (cyan line) in the limit $L \to \infty$. **c** Finite-size scaling of the spin stiffness near the BKT transition, illustrated by its collapse according to the form $\rho_s(t, L) = [1 + 1/(2\ln L + c)]F_\rho(\ln L - a/\sqrt{t - t_{KT}})$, where F_ρ is a scaling function. We extract the parameters $a = 1.1 \pm 0.05$, $c = 0.05 \pm 0.02$, and $t_{KT} = 0.549 \pm 0.002$.

Rather than perform extensive numerical calculations to achieve a higher accuracy, which still would not serve as a proof of exact convergence, we base our discussions, particularly of the multicritical DTAF-TC point, on the analysis of additional symmetries and related models below. At zero field (Fig. 4a), where neither the DS nor the DTAF possesses finite-t order due to symmetry-breaking, using n_t as an effective order parameter reveals a liquid-gas-type transition[16], where the first-order line is terminated by a critical point with Ising universality, and crossover lines (determined from the specific-heat peaks, Supplementary Note 2) appear on both sides of the transition[18].

Ising Criticality

At a fixed low field, where the DTAF has a BKT transition that meets the first-order line at the critical point (Fig. 4b), we investigate the nature of criticality by computing the specific heat as a function of system size, as shown in Fig. 4d. The progressive sharpening of the peak can be characterized by its height, $C_{max}(L)$, which in the inset we find follows precisely the $\ln L$ scaling of Ising universality[16]. Thus we conclude that the BKT transition has no effect on the universality of the critical point in this instance, and we explain this result below.

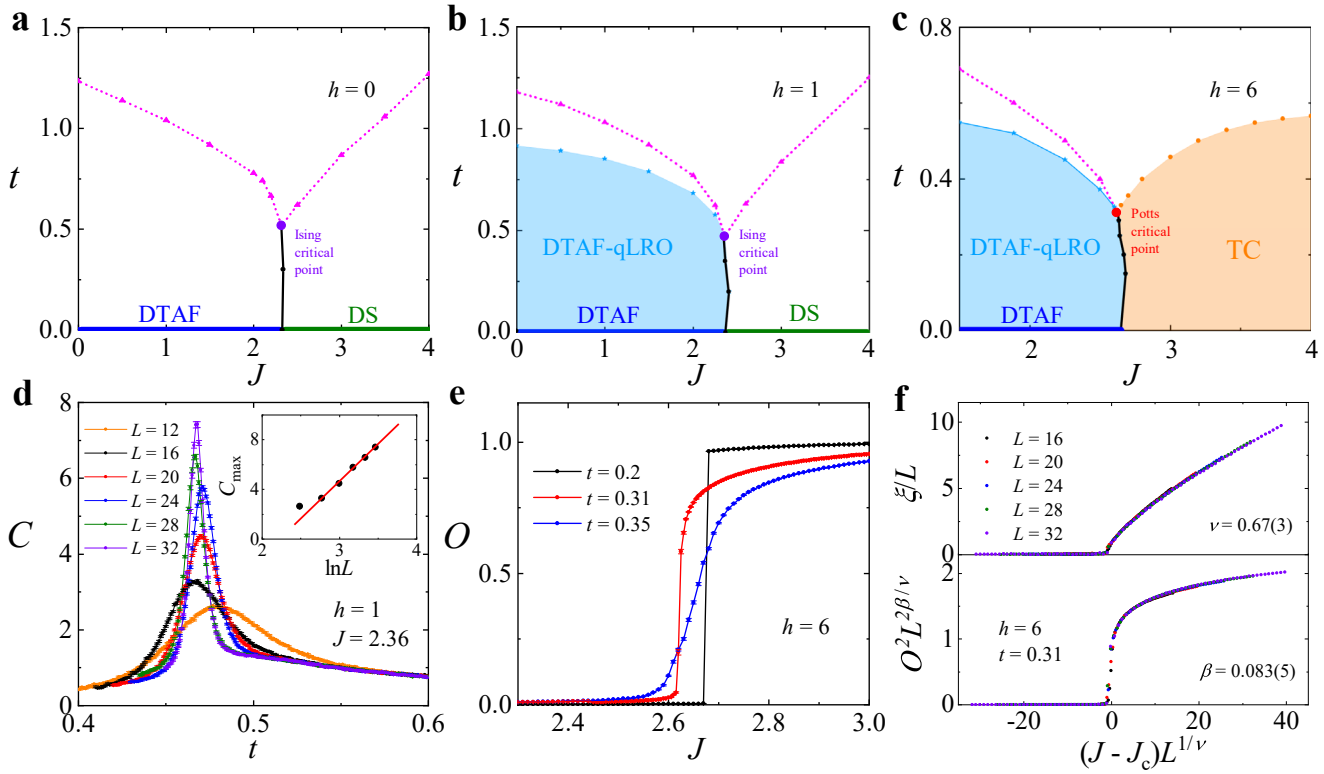

Fig. 4 | Physics of the (multi)critical point. a–c Phase diagrams of the FFB model in the (J, t) plane at $h = 0$ (**a**), $h = 1$ (**b**), and $h = 6$ (**c**). Black lines in each panel mark the first-order transition determined by the discontinuity in the triplet density. Magenta curves show crossover temperatures determined from the specific-heat peaks at each value of h and J. Blue lines and stars mark the BKT transition of the DTAF, below which the system exhibits qLRO. Orange lines and circles show the continuous thermal transition of the TC. Error bars on the phase-boundary points are smaller than the symbol sizes, as we show in Supplementary Figure 5b. At each field, all of the transition and crossover lines meet at a critical point that terminates the line of first-order transitions: this point is located at $(J_c, t_c) = (2.315(1), 0.517(3))$ for $h = 0$[16], $(2.36(1), 0.47(1))$ for $h = 1$, and $(2.624(4), 0.308(5))$ for $h = 6$, and has either Ising (purple circle) or 4-state Potts universality (red circle). **d** Specific heat, $C(t)$, calculated at $J = J_c$ for $h = 1$ using a range of system sizes, L. The sharpening of the peak with increasing L signals a continuous transition and the scaling of the peak value, C_{max}, with $\ln L$ (inset) indicates that the transition in the low-field regime is in the same 2D Ising universality class as the $h = 0$ case. **e** Order parameter, O, of the TC phase calculated with $L = 24$ for $h = 6$ and shown as a function of J near the emergent (multi)critical point for three temperatures below, at, and above t_c. **f** Scaling collapse of the finite-size correlation length, ξ, and the order parameter, O, across the emergent (multi) critical point. The critical exponents estimated from these two types of data collapse are $\nu = 0.67 \pm 0.03$ and $\beta = 0.083 \pm 0.005$, which are fully consistent with 4-state Potts universality.

Emergent Criticality

Turning now to the DTAF-TC transition, in Fig. 4c we show the situation at $h = 6$ and in Supplementary Note 2 we present results elsewhere on this phase boundary. Figure 4e shows explicitly how the discontinuity in the TC order parameter at $t < t_c$ becomes smooth at and above $t_c = 0.31$. At minimum (neglecting the BKT transition), the merging of the discontinuous DTAF-TC line with the continuous thermal transition of the TC phase should change the Ising critical point to a tricritical Ising point. To determine how the universality is altered, in Fig. 4f we consider the scaling collapse of all our finite-L data at t_c for $h = 6$ and extract the critical exponents $\nu = 0.67 \pm 0.03$ and $\beta = 0.083 \pm 0.005$. These values are far from the Ising and tricritical Ising cases, instead corresponding very well to 4-state Potts universality, where $\nu = 2/3$ and $\beta = 1/12$[42].

A priori, this Potts criticality comes as a complete surprise, because the FFB model in a field has no S_4 permutation symmetry, and thus it satisfies all the criteria of an emergent phenomenon. Our discovery of such an exact 4-state Potts universality also appears highly unlikely if the meeting of the three transition lines at a single multicritical point were not exact. To gain further insight, we follow a series of mappings to unveil the underlying symmetries of the system, and summarize the procedure here (a more complete discussion is presented in Supplementary Note 3).

Classical Model

First we map the quantum model of Eq. (2) to a classical model consisting of an O(3) rotor, representing the spin degrees of freedom, coupled to an Ising variable representing the triplon density. It is easy to perform large-scale Monte Carlo simulations of this model, and in Fig. 5a we show that the phase diagram at $h = 6$ is very similar, even semi-quantitatively, to the quantum one (Fig. 4c). A BKT transition arises for the rotors in an applied field and a density-driven Ising transition breaks the sublattice symmetry. Across the critical point where the BKT and Ising transitions meet, we again find $\nu \simeq 2/3$ and $\beta \simeq 1/12$, meaning that the classical model also has 4-state Potts universality.

Spin-Anistropic Model

Next we introduce an Ising-type spin anisotropy, $\Delta > 1$, that breaks the U(1) spin symmetry to Z_2, turning the BKT transition into a thermal Ising transition, below which the system has true LRO that we denote as "x-Ising" in Fig. 5b. In this situation, the two Ising transitions meet at a bicritical point, below which the transition directly from x-Ising to TC is first-order. The bicritical scenario provides a well accepted instance where the three transition lines do meet at a single point, as our numerical results indicate for the FFB model (Fig. 4c). The correlation-length exponent, ν, that we obtain from scaling collapse at the bicritical point varies between 2/3 and 1 with the strength of the spin anisotropy,

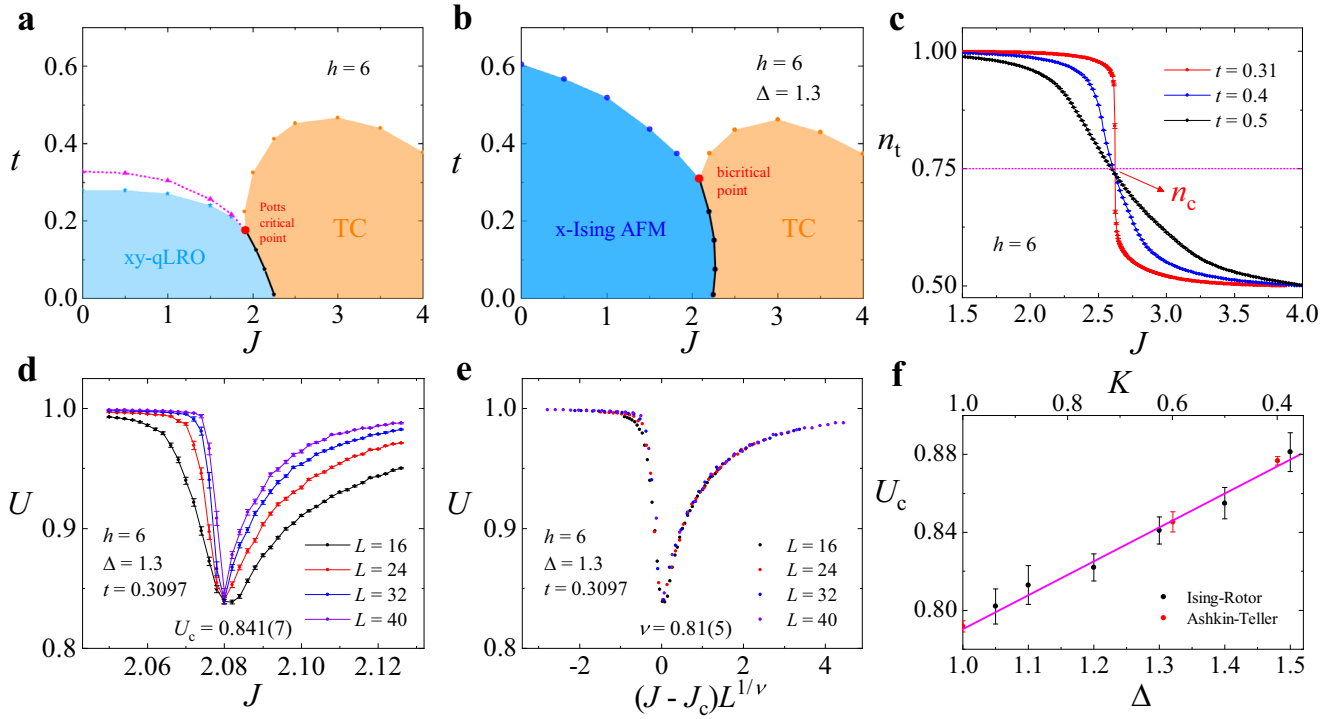

Fig. 5 | Classical model, spin-anisotropic model, and Ashkin-Teller model. **a** Phase diagram of the classical spin-rotor model extracted from the FFB model, shown at $h = 6$. **b** Phase diagram of the classical model with spin anisotropy, shown at $h = 6$ with $\Delta = 1.3$ (weak Ising anisotropy). The qLRO of the DTAF phase becomes a true LRO with a thermal Ising transition occurring at a rather higher ordering temperature. Because the TC phase retains its Ising transition, the emergent critical point becomes a bicritical point (red circle) where the two Ising transition lines meet at $(J_c, t_c) = (2.0792(14), 0.3097(8))$. Error bars on the phase-boundary points in both panels are smaller than the symbol sizes. **c** Triplet density, n_t, computed for $L = 24$ and shown as a function of J for various temperatures at $h = 6$. $n_t = 0.75$ at the multicritical point and reflects the approximate particle-hole symmetry between the DTAF and TC phases at their transition. **d** Binder cumulant, U, computed as a function of J across the bicritical point with $h = 6$ and $\Delta = 1.3$ for a range of system sizes. $J_c = 2.0792 \pm 0.0014$ is determined from the touching point of the Binder-cumulant curves. **e** Collapse of the Binder-cumulant data shown in panel d, from which we estimate the non-universal critical exponent $\nu = 0.81 \pm 0.05$. **f** Critical value of the Binder cumulant at the bicritical point, U_c (black circles), shown as a function of the spin anisotropy. For comparison we show U_c values at the critical points of the Ashkin-Teller model (ATM, red circles). The magenta line is a linear fit which shows that extrapolating U_c to the spin-isotropic limit ($\Delta = 1$) gives good agreement with the critical value obtained at $K/J = 1$ in the ATM, where this model has 4-state Potts universality.

as we show in Supplementary Note 3, and thus the anisotropic classical model has non-universal behavior.

Ashkin-Teller Model

Because both the DTAF and TC phases break the sublattice symmetry, each has two degenerate configurations, and in total four ground-state configurations are degenerate at the transition. Here the triplon density drops from $n_t = 1$ in the DTAF to $n_t = 1/2$ in the TC, and the evolution of n_t with J across the emerging critical point indicates a particle-hole symmetry about $n_t = 3/4$ (Fig. 5c). Defining the Ising variables σ_i, associated with the sublattice symmetry, and η_i, associated with the particle-hole symmetry, the Ising variable $\tau_i = \sigma_i\eta_i$ obeys the relations $\tau \to -\sigma$ and $\sigma \to -\tau$ under spin inversion. With these variables we construct the minimal effective model that should describe the critical properties around the emerging critical point in the form

$$H_{\text{eff}} = -J\sum_{i,j}(\sigma_i\sigma_j + \tau_i\tau_j) - K\sum_{i,j}(\sigma_i\sigma_j)(\tau_i\tau_j), \tag{3}$$

as discussed in detail in Supplementary Note 3. This $Z_2 \times Z_2 \times Z_2$-symmetric model is precisely the Ashkin-Teller model (ATM). It is well known[43] that the ATM exhibits non-universal exponents along the critical line obtained for $0 < K/J < 1$, with Ising universality at $K/J = 0$ and a higher Potts universality at $K/J = 1$.

To analyse the correspondence between this ATM and the classical model with variable spin anisotropy, we define a composite order parameter, $O_b^2 = O_x^2 + O_{TC}^2$, that contains the order of both the x-Ising and TC phases (Supplementary Note 3C). We then consider the Binder cumulant associated with O_b, $U = 2(1 - \langle O_b^4\rangle/2\langle O_b^2\rangle^2)$, which has the property that $U \to 1$ deep in both ordered phases, but dips across the bicritical point. Figure 5d shows this evolution of U for a range of system sizes, from whose touching point we determine both the location of the bicritical point and the value U_c. Because of its dimensionless nature, U_c should also reflect the universality of the critical point[44–47], and the scaling collapse shown in Fig. 5e presents an accurate means of extracting ν. For the spin-anisotropic model, we find that both U_c and ν vary with the anisotropy Δ, exhibiting a non-universal evolution such that ν at the bicritical point varies between 1 and 2/3, signalling a continuous change between Ising and 4-state Potts universality. The monotonic dependence of U_c on Δ, shown in Fig. 5f, compares exactly with the K/J scaling of the ATM, and its extrapolated value as $\Delta \to 1$ agrees well with the value $U_c \to 0.792 \pm 0.003$ found for the ATM at the Potts point[47].

Discussion

We have presented the global phase diagram of the FFB Heisenberg model in an applied magnetic field, showing how the field allows systematic control over the phase competition. We have explained the rich variety of phase transitions and (multi)critical lines or points, and found numerical evidence for a striking example of emerging critical behavior. This emergent 4-state Potts universality, arising along the line of multicritical points where the BKT transition of the DTAF and the Ising one of the TC phase meet, implies that the multicritical system has a higher S_4 permutation symmetry

that the microscopic spin model does not possess. This result is clearly different from previous studies of transitions between BKT and Ising phases, such as the well known FFXY [$U(1) \otimes Z_2$] model[48], of anisotropic Heisenberg spin models[49], and of higher symmetries emerging from combined Ising order parameters[12,13]. In the FFB, a symmetry analysis reveals an additional particle-hole symmetry that lies beyond all of these models and can be used to map the critical system to an effective ATM. The generic ATM has a wide parameter regime where one line of critical points has nonuniversal and continuously varying exponents, as we find in the model with spin anisotropy. In the isotropic limit, where the spin symmetry is enhanced to U(1), we expect 4-state Potts universality (i.e. an enhanced S_4 symmetry), because the Potts point is the only multicritical point with enhanced symmetry in the ATM[50]. Precisely how this effective S_4 symmetry emerges in the critical behavior as the spin symmetry is restored to U(1) is a well defined problem that deserves further exploration in the expanding field of emergent phenomena.

We found at low fields that the BKT phase of the DTAF has no effect on the Ising nature of the zero-field critical point. This result is explained by the fact that the phase mode associated with the BKT transition couples only marginally to the Ising variable (the triplet density, which is an amplitude mode), as we discuss in Supplementary Note 3. At fields high enough to create the TC phase, once again the BKT nature of the DTAF plays no role in determining the properties, including the emergent Potts universality, of the multicritical line: our construction of the ATM relied on the three symmetries of the system, but not on the presence of qLRO when the spin anisotropy is removed.

It is instructive to consider our results in the context of the conformally invariant field theories (CFTs) describing criticality in two-dimensional systems[51]. In CFTs with central charge $c < 1$, c may only take discrete values, which characterize critical points of different universalities, including the Ising transition ($c = 1/2$). In $c \geqslant 1$ CFTs, on the other hand, models with continuously varying critical exponents are allowed, and this makes the space of these CFTs very rich. In particular, the family of $c = 1$ CFTs includes many models that can be distinguished by their compactification radius on a circle or an orbifold[52]. As examples, the BKT transition is described by the $c = 1$ CFT on a torus, whereas an ATM with $K \leqslant J$ is described by the $c = 1$ CFT on an orbifold, whose compactification radius changes over a continuous range of values. Our derivation of the effective model representing the physics of the FFB makes clear that it is the emergent particle-hole symmetry which provides the third Z_2 symmetry elevating the model to an ATM, and thus conferring the orbifold character. The effect of the BKT transition on the ATM is expected to be marginal because it does not alter either the central charge or the orbifold nature. More generally, the unexpected emergent 4-state Potts symmetry of the multicritical line offers the possible realization in frustrated quantum magnetic materials of a $c = 1$ orbifold CFT previously discussed in physics only in the context of fractional quantum Hall states[53].

We expect that the multicritical points, emergent critical properties, and QCEP we find in the FFB model are directly relevant to a number of dimerized and frustrated quantum magnetic materials. The compound $Ba_2CoSi_2O_6Cl_2$ was found to have the FFB geometry[54], and its magnetic properties were studied using the FFB model with a strong in-plane spin anisotropy[35]. Thus one might anticipate exploring some of the FFB phase diagram under the combined application of magnetic field and hydrostatic pressure in this material. The zero-field Ising critical point of the FFB has been found in the orthogonal-dimer geometry of $SrCu_2(BO_3)_2$[21], which has the same quality of ideal frustration. Both the plaquette phase of this system and the TC phase of the FFB model have broken Z_2 symmetry, allowing finite-temperature order, and hence our results for the TC phase boundaries should help to interpret the transitions into the plaquette-solid and the putative plaquette-liquid phases of $SrCu_2(BO_3)_2$. Of particular concern is the issue of whether an isolated Ising critical point[21] can persist at finite fields, or whether more complex (multi)critical behavior should set in[28], as we find at the DTAF-TC transition in the FFB. At applied magnetic fields above 20 T, $SrCu_2(BO_3)_2$ exhibits a spin-nematic phase[24] followed by a cascade of fractional magnetization-plateau states[25], and at higher pressures is believed to show the AF phase of the SSM above the plaquette phase[14]. While these phases lie somewhat beyond those of the FFB model, they do raise the prospect of multiple opportunities to search for emergent critical behavior along the associated phase-transition lines[55]. Thus we expect our more global results, concerning symmetries and effective models, to provide a useful foundation for new theoretical and experimental studies of criticality and emergent phenomena in $SrCu_2(BO_3)_2$.

Methods

iPESS

We study the quantum phase diagram of the FFB model using the PESS tensor-network method[32]. The simplex basis allows a highly efficient encoding of the entanglement in frustrated quantum spin systems, and its construction is described in Supplementary Note 1. The lattice translation symmetry is used to work on a spatially infinite system and the ground state is found by evolution in imaginary time, for which a simple-update method is sufficient in the FFB. Because three of the four ground states are known exactly, detailed calculations pushing the limits of the truncation parameter (D, the tensor bond dimension) are not required to achieve accurate convergence (Supplementary Note 1).

QMC

As noted above, the total absence of a sign problem in the fully frustrated model ($J_\parallel = J_\times$) makes SSE QMC simulations possible on large systems and at low temperatures. To extract the maximum accuracy from our simulations, in particular for the determination of critical points and exponents, we exploit the finite-size scaling properties of the known phases. Error bars shown on all QMC data represent the standard deviation (s.d.).

The transition to the TC phase is studied by defining the dimer-triplet correlation function

$$R(\vec{k}) = L^{-2} \sum_{ij} e^{i\vec{k}\cdot(\vec{r}_i - \vec{r}_j)} \left\langle \left(T_i^2 - 1\right)\left(T_j^2 - 1\right)\right\rangle, \tag{4}$$

from which we obtain the correlation length

$$\xi = \frac{2\pi}{L}\sqrt{R(\vec{Q})/R(\vec{Q} + \delta\vec{Q}) - 1} \tag{5}$$

and the order parameter

$$O^2 = R(\vec{Q})/L^2, \tag{6}$$

where $\vec{Q} = (\pi, \pi)$ is the ordering wavevector and $\delta\vec{Q} = (2\pi/L, 0)$. We obtain the critical exponents by establishing the scaling collapse of both quantities in the forms[41]

$$\xi = LF_{\xi,g}\left(|g|L^{1/\nu}\right), \tag{7}$$

$$O^2 = L^{2\beta/\nu}F_{O,g}\left(|g|L^{1/\nu}\right), \tag{8}$$

where $|g|$ denotes the three quantities $|J - J_c|$, $|h - h_c|$, and $|t - t_c|$ that we use to effect a systematic approach to the critical points when the other variables are fixed to their critical values. F denotes a single function that describes all the data when scaled in this way, allowing a highly accurate determination of the critical exponents.

To study the BKT transition, we calculate the spin stiffness from the expression $\rho_s = \frac{1}{2}t\langle w_x^2 + w_y^2\rangle$, in which $w_\alpha = \sum_b (N_{b,\alpha}^+ - N_{b,\alpha}^-)/L$ with α denoting the direction x or y and $N_{b,\alpha}^\pm$ expressing the number of operators $T_{i(b)}^\pm T_{j(b)}^\mp$ associated with bond b in direction α appearing in the QMC

operator sequence[41]. The system size can again be used to effect a scaling collapse of ρ_s to the form employed in Fig. 3[40,41],

$$\rho_s = \frac{2t_{KT}}{\pi}\left[1+\frac{1}{2\ln L + c}\right]F_\rho\left(\ln L - a/\sqrt{t-t_{KT}}\right), \quad (9)$$

where a and c are fitting parameters and $F_\rho(t, L)$ is a single scaling function. This collapse allows an accurate determination of the BKT transition temperature, t_{KT}.

Data availability

The data that support the findings of this study are available from the corresponding authors upon reasonable request.

Code availability

The code that supports the findings of this study is available from the corresponding authors upon reasonable request.

Received: 26 October 2023; Accepted: 26 February 2024;
Published online: 09 March 2024

References

1. Zinn-Justin, J. *Quantum Field Theory and Critical Phenomena*. (Oxford University Press, Oxford, 2002).
2. Savary, L. & Balents, L. Quantum spin liquids: a review. *Rep. Prog. Phys.* **80**, 016502 (2017).
3. Sachdev, S. *Quantum Phase Transitions, Second Edition*. (Cambridge University Press, Cambridge, 2011).
4. Zapf, V., Jaime, M. & Batista, C. Bose-Einstein condensation in quantum magnets. *Rev. Mod. Phys.* **86**, 563 (2014).
5. Merchant, P. et al. Quantum and classical criticality in a dimerized quantum antiferromagnet. *Nat. Phys.* **10**, 373–379 (2014).
6. Senthil, T., Vishwanath, A., Balents, L., Sachdev, S. & Fisher, M. P. A. Deconfined Quantum Critical Points. *Science* **303**, 1490–1494 (2004).
7. Senthil, T., Balents, L., Sachdev, S., Vishwanath, A. & Fisher, M. P. A. Quantum criticality beyond the Landau-Ginzburg-Wilson paradigm. *Phys. Rev. B* **70**, 144407 (2004).
8. Zhao, B., Takahashi, J. & Sandvik, A. W. Multicritical Deconfined Quantum Criticality and Lifshitz Point of a Helical Valence-Bond Phase. *Phys. Rev. Lett.* **125**, 257204 (2020).
9. Lu, D.-C., Xu, C. & You, Y.-Z. Self-duality protected multi-criticality in deconfined quantum phase transitions. *Phys. Rev. B* **104**, 205142 (2021).
10. Shao, H., Guo, W. & Sandvik, A. W. Quantum criticality with two length scales. *Science* **352**, 213–216 (2016).
11. Zhao, B., Weinberg, P. & Sandvik, A. Symmetry-enhanced discontinuous phase transition in a two-dimensional quantum magnet. *Nat. Phys.* **15**, 678 (2019).
12. Zhu, G.-Y. & Zhang, G.-M. Gapless Coulomb State Emerging from a Self-Dual Topological Tensor-Network State. *Phys. Rev. Lett.* **122**, 176401 (2019).
13. Schuler, M., Henry, L.-P., Lu, Y.-M. & Läuchli, A. M. Emergent XY* transition driven by symmetry fractionalization and anyon condensation. *SciPost Phys.* **14**, 001 (2023).
14. Zayed, M. et al. 4-spin plaquette singlet state in the Shastry-Sutherland compound $SrCu_2(BO_3)_2$. *Nat. Phys.* **13**, 962 (2017).
15. Yu, R. et al. Bose glass and Mott glass of quasiparticles in a doped quantum magnet. *Nature* **489**, 379 (2012).
16. Stapmanns, J. et al. Thermal Critical Points and Quantum Critical End Point in the Frustrated Bilayer Heisenberg Antiferromagnet. *Phys. Rev. Lett.* **121**, 127201 (2018).
17. Chaikin, P. M. & Lubensky, T. C. *Principles of Condensed Matter Physics*. (Cambridge University Press, Cambridge, 1995).
18. Weber, L. et al. Quantum Monte Carlo simulations in the trimer basis: first-order transitions and thermal critical points in frustrated trilayer magnets. *SciPost Phys.* **12**, 054 (2022).
19. Weber, L., Fache, A. Y. D., Mila, F. & Wessel, S. Thermal critical points from competing singlet formations in fully frustrated bilayer antiferromagnets. *Phys. Rev. B* **106**, 235128 (2022).
20. Strečka, J. et al. Thermal first-order phase transitions, Ising critical points, and reentrance in the Ising-Heisenberg model on the diamond-decorated square lattice in a magnetic field. *Phys. Rev. B* **107**, 134402 (2023).
21. Larrea Jiménez, J. et al. A quantum magnetic analogue to the critical point of water. *Nature* **592**, 370 (2021).
22. Shastry, B. S. & Sutherland, B. Exact ground state of a quantum mechanical antiferromagnet. *Physica B+C* **108**, 1069–1070 (1981).
23. Kageyama, H. et al. Exact Dimer Ground State and Quantized Magnetization Plateaus in the Two-Dimensional Spin System $SrCu_2(BO_3)_2$. *Phys. Rev. Lett.* **82**, 3168 (1999).
24. Fogh, E. et al. Field-induced bound-state condensation and spin-nematic phase in $SrCu_2(BO_3)_2$ revealed by neutron scattering up to 25.9 T. *Nat. Commun.* **15**, 442 (2024).
25. Matsuda, Y. H. et al. Magnetization of $SrCu_2(BO_3)_2$ in Ultrahigh Magnetic Fields up to 118 T. *Phys. Rev. Lett.* **111**, 137204 (2013).
26. Lee, J. Y., You, Y.-Z., Sachdev, S. & Vishwanath, A. Signatures of a Deconfined Phase Transition on the Shastry-Sutherland Lattice: Applications to Quantum Critical $SrCu_2(BO_3)_2$. *Phys. Rev. X* **9**, 041037 (2019).
27. Yang, J., Sandvik, A. W. & Wang, L. Quantum criticality and spin-liquid phase in the Shastry-Sutherland model. *Phys. Rev. B* **105**, L060409 (2022).
28. Cui, Y. et al. Proximate deconfined quantum critical point in $SrCu_2(BO_3)_2$. *Science* **380**, 1179–1184 (2023).
29. Alet, F., Damle, K. & Pujari, S. Sign-Problem-Free Monte Carlo Simulation of Certain Frustrated Quantum Magnets. *Phys. Rev. Lett.* **117**, 197203 (2016).
30. Honecker, A. et al. Thermodynamic properties of highly frustrated quantum spin ladders: Influence of many-particle bound states. *Phys. Rev. B* **93**, 054408 (2016).
31. Syljuåsen, O. F. & Sandvik, A. W. Quantum Monte Carlo with directed loops. *Phys. Rev. E* **66**, 046701 (2002).
32. Xie, Z. Y. et al. Tensor Renormalization of Quantum Many-Body Systems Using Projected Entangled Simplex States. *Phys. Rev. X* **4**, 011025 (2014).
33. Richter, J., Derzhko, O. & Krokhmalskii, T. Finite-temperature order-disorder phase transition in a frustrated bilayer quantum Heisenberg antiferromagnet in strong magnetic fields. *Phys. Rev. B* **74**, 144430 (2006).
34. Derzhko, O., Krokhmalskii, T. & Richter, J. Emergent Ising degrees of freedom in frustrated two-leg ladder and bilayer $s = \frac{1}{2}$ Heisenberg antiferromagnets. *Phys. Rev. B* **82**, 214412 (2010).
35. Richter, J., Krupnitska, O., Baliha, V., Krokhmalskii, T. & Derzhko, O. Thermodynamic properties of $Ba_2CoSi_2O_6Cl_2$ in a strong magnetic field: Realization of flat-band physics in a highly frustrated quantum magnet. *Phys. Rev. B* **97**, 024405 (2018).
36. Fisher, M. E. & Upton, P. J. Universality and interfaces at critical end points. *Phys. Rev. Lett.* **65**, 2402 (1990).
37. Fisher, M. E. & Barbosa, M. C. Phase boundaries near critical end points. I. Thermodynamics and universality. *Phys. Rev. B* **43**, 11177 (1991).
38. Berezinskii, V. L. Destruction of Long-range Order in One-dimensional and Two-dimensional Systems Possessing a Continuous Symmetry Group. II. Quantum Systems. *Sov. Phys. JETP* **34**, 610 (1972).
39. Kosterlitz, J. M. & Thouless, D. J. Long range order and metastability in two dimensional solids and superfluids. (Application of dislocation theory). *J. Phys. C: Solid State Phys.* **5**, L124 (1972).

40. Weber, H. & Minnhagen, P. Monte Carlo determination of the critical temperature for the two-dimensional XY model. *Phys. Rev. B* **37**, 5986 (1988).
41. Sandvik, A. W. Computational Studies of Quantum Spin Systems. *AIP Conf. Proc.* **1297**, 135–338 (2010).
42. Wu, F. Y. The Potts model. *Rev. Mod. Phys.* **54**, 235 (1982).
43. Wiseman, S. & Domany, E. Cluster method for the Ashkin-Teller model. *Phys. Rev. E* **48**, 4080 (1993).
44. Goldenfeld, N. *Lectures on Phase Transitions and the Renormalization Group*. (Addison-Wesley, Reading, 1992).
45. Chen, X. S. & Dohm, V. Nonuniversal finite-size scaling in anisotropic systems. *Phys. Rev. E* **70**, 056136 (2004).
46. Selke, W. & Shchur, L. N. Critical Binder cumulant in two-dimensional anisotropic Ising models. *J. Phys. A* **38**, L739 (2005).
47. Jin, S., Sen, A. & Sandvik, A. W. Ashkin-Teller Criticality and Pseudo-First-Order Behavior in a Frustrated Ising Model on the Square Lattice. *Phys. Rev. Lett.* **108**, 045702 (2012).
48. Song, F.-F. & Zhang, G.-M. Tensor network approach to the two-dimensional fully frustrated XY model and a chiral ordered phase. *Phys. Rev. B* **105**, 134516 (2022).
49. Holtschneider, M., Wessel, S. & Selke, W. Classical and quantum two-dimensional anisotropic Heisenberg antiferromagnets. *Phys. Rev. B* **75**, 224417 (2007).
50. Dijkgraaf, R., Verlinde, E. & Verlinde, H. $c = 1$ conformal field theories on Riemann surfaces. *Commun. Math. Phys.* **115**, 649–690 (1988).
51. Friedan, D., Qiu, Z. & Shenker, S. Conformal Invariance, Unitarity, and Critical Exponents in Two Dimensions. *Phys. Rev. Lett.* **52**, 1575 (1984).
52. Ginsparg, P. C. Curiosities at $c = 1$. *Nucl. Phys. B* **295**, 153 (1988).
53. Tam, P. M., Hu, Y. & Kane, C. L. Coupled wire model of $Z_2 \times Z_2$ orbifold quantum Hall states. *Phys. Rev. B* **101**, 125104 (2020).
54. Tanaka, H. et al. Almost Perfect Frustration in the Dimer Magnet $Ba_2CoSi_2O_6Cl_2$. *J. Phys. Soc. Jpn.* **83**, 103701 (2014).
55. Shi, Z. et al. Discovery of quantum phases in the Shastry-Sutherland compound $SrCu_2(BO_3)_2$ under extreme conditions of field and pressure. *Nat. Commun.* **13**, 2301 (2022).

Acknowledgements

We thank F. Mila, Y. Wan, Y. Wang, S. Wessel, and W. Yu for helpful discussions. This work was supported in part by the National Natural Science Foundation of China under Grant Nos. 12334008, 12174441, 11974396, and 12188101. We acknowledge the Physical Laboratory of High-Performance Computing at Renmin University of China for the provision of computational resources and the National Supercomputer Center in Guangzhou for the use of the Tianhe-2 supercomputer.

Author contributions

The project was conceived by B.N. and R.Y. QMC calculations were performed by Y.F. and PESS calculations by N.X. Theoretical interpretation was provided by Y.F., C.L., B.N. and R.Y. The manuscript was written by Y.F., B.N. and R.Y. with contributions from all the authors.

Competing interests

The authors declare no competing interests.

Additional information

Supplementary information The online version contains supplementary material available at https://doi.org/10.1038/s41535-024-00636-4.

Correspondence and requests for materials should be addressed to Bruce Normand or Rong Yu.